Published in: Physica C-Superconductivity and its Applications (2003), vol. 387, iss. 1-2, pp. 191-197
Status: Postprint (Author's version)

Magneto-transport study of Nb-doped Bi/Pb2223 superconductor

Marek Pękala [a], Jan Mucha [b], Rudi Cloots [c], Jean-François Fagnard [d],
Philippe Vanderbemden [d], Marcel Ausloos [e]

[a] *Department of Chemistry, University of Warsaw, Aleja Żwirki i Wigury 101, 02-089 Warszawa, Poland*
[b] *Institute of Low Temperature and Structural Research of the Polish Academy of Sciences, 50-950 Wroclaw, Poland*
[c] *S.U.P.R.A.S., Institute of Chemistry B6, University of Liège, Sart Tilman, B-4000 Liège, Belgium*
[d] *S.U.P.R.A.S., Montefiore Institute of Electricity B28, University of Liège, Sart Tilman, B-4000 Liège, Belgium*
[e] *S.U.P.R.A.S., Institute of Physics B5, University of Liège, Sart Tilman, B-4000 Liège, Belgium*

Abstract

The magneto-transport properties of $Bi_{1.5}Pb_{0.4}Nb_{0.1}Sr_2Ca_2Cu_3O_{10-x}$ polycrystalline, superconducting ceramic are reported. The material was found to be chemically homogeneous and partially textured. The mixed state properties were investigated by measuring the electrical resistivity, longitudinal and transverse (Nernst effect) thermoelectric power, and thermal conductivity. The magnetization and AC susceptibility measurements were also performed. The variation of these characteristics for magnetic fields up to 5 T are discussed and compared to those of the zero field case. The transport entropy and thermal Hall angle are extracted and quantitatively compared to previously reported data of closely related systems.

Keywords: Nernst effect ; thermoelectric power ; thermal conductivity

1. Introduction

Among the Bi-based high critical temperature superconducting cuprate ceramics Bi-2223 is, likely, the most interesting for practical applications. It has a high T_c and is non-toxic. However, it is rarely found as a pure, single-phase material. It is also difficult to texture. There has been much work done to try to improve the synthesis techniques for these materials. This is the reason why we previously developed a process like the "glassy phase-crystalline precursor approach" [1-3]. By modifying the initial stoichiometry, preceded by quenching to a glass phase, and by modifying the crystalline precursor, which initiates nucleation, an optimum process was designed that leads to nearly single-phase "high quality" 2223 materials. It was found that the presence of CaO and CuO in the glassy precursor is beneficial for the growth of the 2223 phase. On the contrary, SrO seems to delay the growth of this phase [1-3].

Some other work has been presented for an original synthesis technique which results in high-quality (from a technological point of view) Bi-based 2223 materials when $BaZrO_3$ substrates and the non-conventional glassy matrix method are used [4]. The effect of $BaZrO_3$ additions on the microstructure and physical properties of melt-textured Y-123 superconducting materials has also been discussed in Refs. [5,6].

Many groups applied various approaches in order to enhance the quality of the bismuth-based superconductors, for which an increase of critical current density was especially sought. The superconducting transition temperature of the Pb-substituted Bi-2223 phase can rise to 125 K via Ba substitution [7]. This value is the highest for Bi-based cuprate superconductors. Moreover, substitution of Nb for Bi is known to promote the formation of the Bi-2223 phase [8,9]. In fact, Nb, like Pb, can also improve the intergrain connectivity. However, the physical properties of such systems are not well known. There are very few reports of high temperature superconductors doped with elements from the fifth column of periodic table. We have performed detailed magneto-transport investigations of niobium doped Bi/ Pb2223 superconductors. Some discussion is presented here in view of similar data on related systems [10,11].

2. Sample preparation and characterization

Polycrystalline samples with an intended composition of $Bi_{1.5}Pb_{0.4}Nb_{0.1}Sr_2Ca_2Cu_3O_{10-x}$ were prepared by solid state reaction of stoichiometric amounts of high-purity metallic oxides. Regular grinding, sintering at 840 °C, and rapid cooling followed initial calcination. In order to perform magnetic field texturing, ions with a magnetic moment cannot be introduced in the Bi-2223 phase. Thus, some moderate pressure was applied to improve the mutual ordering of grains. X-ray diffraction data shows that the prevalent phase in the samples was Bi/Pb2223. The remaining fraction of the sample consisted of the Bi-2212 phase (<5%), and was concentrated in the intergrain regions.

An SEM analysis of the polycrystalline samples showed platelet grains amassed along the *c*-direction. Such a partial orientation of planar-like grains should have a twofold influence on the properties of the samples. First, it

should improve the connectivity between grains along the c-direction. Secondly, it should reduce the amount of skewed grains within the volume between adjacent platelet grains, i.e. there should be a smaller amount of *c*-oriented grains between planar-oriented grains when compared to the case of non-textured materials with random grain orientation. The grain thickness is of the order of 25 μm, but their "upper face" can present areas as large as 200 x 200 μm. An EDX analysis was performed over different spots of the sample, with a Si-Li detector, for Ca-K, Cu-K, Sr-L and Bi-M line standards. The Bi peak, in this case, conceals the Nb and Pb peaks. However, the Sr, Ca, and Cu peaks are well distinguished. Some minute indication of Al suggests contamination during the synthesis process. Some CaO and CuO phases are occasionally found locally as well. However, the homogeneity of the composition is relatively uniform, from location to location, within admissible error bars (on the order of <3% and assuming a crystallographic unit cell made of 32 anions). The chemical formula calculated $(Bi,Pb,Nb)_2(Sr,Ca)_4$-Cu_3O_{10} is found to be very close to the system intended.

3. Magnetic and transport measurements

The electrical and thermal transport properties were measured in a closed cycle refrigerator. The sample temperature was stabilized to within an accuracy of better than 0.01 K. The electrical resistivity was measured with a four point probe, DC method and a current of 1-10 mA. The applied current density was ≈0.1 A/cm^2. The thermoelectric power, the Nernst effect, and the thermal conductivity were measured by creating a temperature gradient with a small 10 mW heater. The magnetic field applied was perpendicular to the temperature gradient.

The AC susceptibility was measured at a frequency of 1053 Hz and a field amplitude of 10 Gs. The DC magnetization was measured with a 50 Gs/s magnetic field sweep rate and a temperature sweep rate of 0.5 K/min.

4. Results

4.1. Electrical resistivity

The electrical resistivity, $\rho(T)$, of polycrystalline samples is of the order of 10^{-5} Ωm at room temperature, and is comparable to the *ab*-plane resistivity of single crystals. This relatively low resistivity of the samples studied likely indicates that the partial ordering of platelet shaped grains improves the intergrain connectivity in the *ab*-plane and short circuits the *c*-axis connections of comparable superconductors with chaotically spread grains. Between 140 and 300 K, the electrical resistivity varies nearly in proportion to the temperature (Fig. 1a) at a mean rate of 3 x 10^{-8} Ω/K.

The electrical resistivity, in the absence of an external magnetic field, falls to zero at 109 K in a narrow temperature interval, without any apparent break in slope (Fig. 1b). This confirms the high quality and homogeneity of samples exhibiting good intergrain connectivity. However, an external magnetic field remarkably broadens the superconducting transition interval, which can be as large as 60 K at B = 8 T. With such large magnetic fields the density of vortices is high. Vortex motion resistance thus arises from two contributions; one associated to friction with a drag effect on a single vortex (flux flow viscosity triggered by the electrical current), and another from vortex-vortex interaction. The latter contributes to some viscous effect, due to vortex entanglement, and is responsible for the fact that the results of the diffusion-like motion of vortices are markedly different across various defect regimes, thereby leading to a complicated $R(T,H)$. Therefore, the vortex viscosity,

$$\eta(T) = \Phi_0 B_{c2}(T)/\rho(T) \qquad (1)$$

calculated from the electrical resistivity, increases when passing from high to low temperatures [12]. The magnitude of the vortex viscosity is obviously higher in stronger magnetic fields, reflecting the increasing intervortex interaction at high vortex density.

Fig. 1. *(a) Temperature variation of the electrical resistance measured in various external magnetic fields (in the whole region of the measured temperatures), (b) Temperature variation of the electrical resistance is shown in external magnetic fields of various strength (below the transition temperature).*

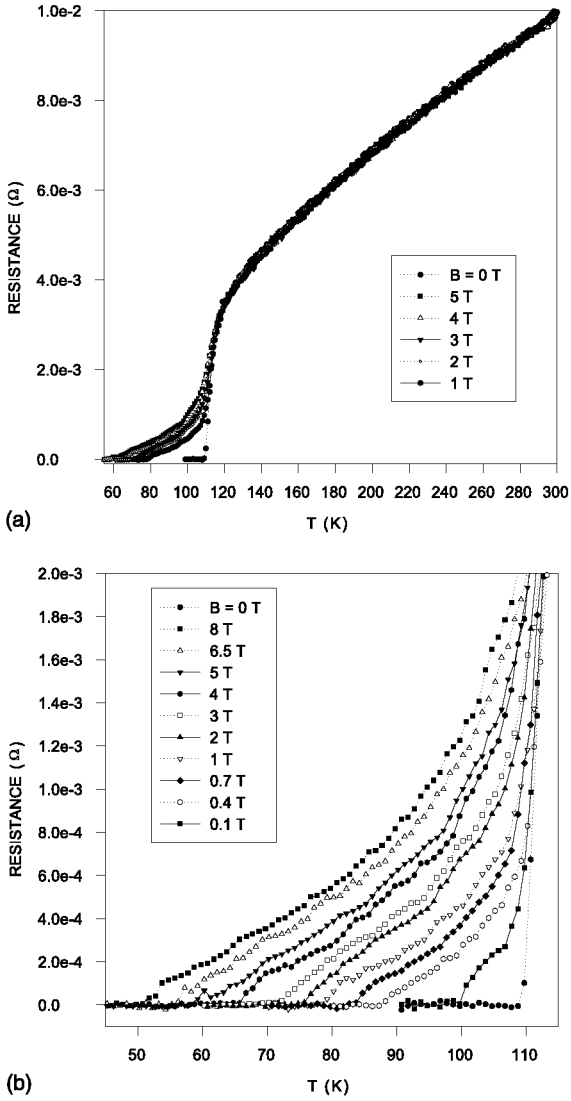

4.2. Thermoelectric power

In the normal state, above 140 K where it has a maximum, the thermoelectric power (TEP) varies approximately linearly with temperature (Fig. 2a), and has a mean slope of -4 x 10^{-8} V/K^2. Deviations from a linear variation appear below 150 K. In the absence of an external magnetic field, the TEP is about 2 x 10^{-6} V/K at room temperature. TEP is known to be a sensitive probe of the oxygen doping, which is closely related to the critical temperature and the absolute value of thermoelectric power, Q_{RT}, at room temperature. The room temperature value of TEP, as low as 2 μV/K, confirms that the sample is optimally doped with about 0.16 hole per copper atom in the CuO_2 layer [13]. The width of the transition interval is about 15 K in zero field (Fig. 2b). The mixed state extends gradually under increasing magnetic fields and disappears (TEP = 0) around 70 K at B = 5 T.

4.3. Nernst effect

The mixed state Nernst signal is initially established just below 115-120 K (Fig. 3), rises abruptly in a relatively narrow interval of about 5 K, reaches a maximum around 110 K, and then diminishes at lower temperatures. The Nernst signal vanishes below ≈77 K at 5 T.

The thermal Hall angle, α_{th}, determining the angle between the vortex velocity and the temperature gradient was calculated as

Published in: Physica C-Superconductivity and its Applications (2003), vol. 387, iss. 1-2, pp. 191-197
Status: Postprint (Author's version)

$$\alpha_{th} = \arctan(NB/Q) \qquad (2)$$

where N and Q are the Nernst and longitudinal thermoelectric signals. Fig. 4 shows that, for a 1 T field, α_{th} attains values of about 75°, whereas at fields of the order of 4-5 T this angles varies between 20° and 25°. Moreover, the entropy

$$S_{\varphi}(T) = \Phi_0 N/\rho \qquad (3)$$

transported by vortices was calculated as a function of temperature and is shown in Fig. 5.

The transport entropy abruptly rises with decreasing temperature to just below the transition temperature. It attains a maximum value at about 107 K, and is almost independent of the magnetic field strength. The magnitude of S_{φ} increases mono-tonically with the magnetic field strength.

Fig. 2. *(a) Temperature variation of the thermoelectric power measured in various external magnetic fields (in the whole region of the measured temperatures), (b) Temperature variation of the thermoelectric power is shown in external magnetic fields of various strength (below the transition temperature).*

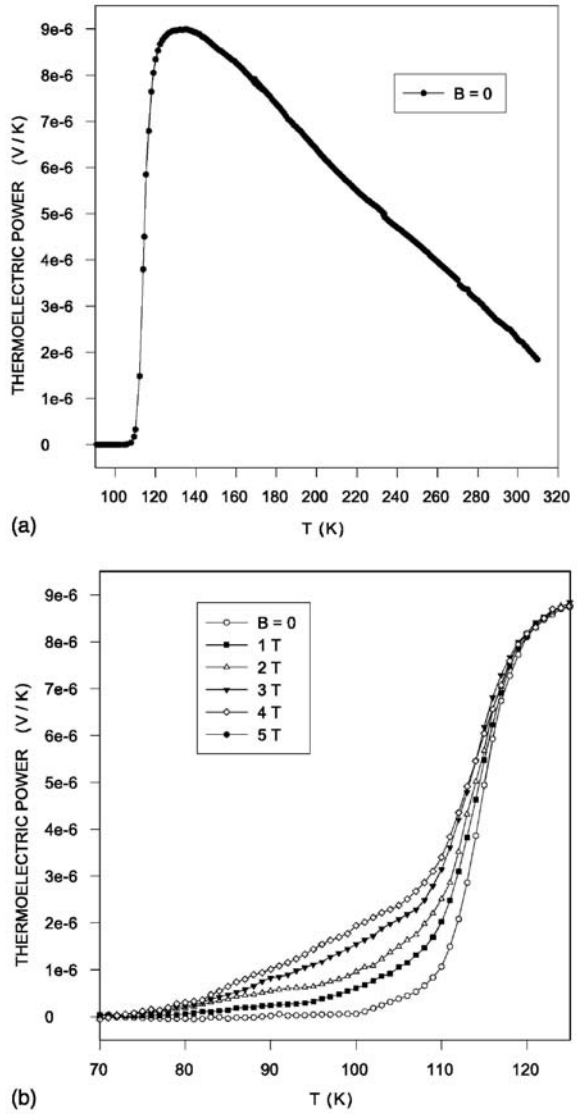

Fig. 3. *Temperature variation of the Nernst signal measured in various magnetic fields.*

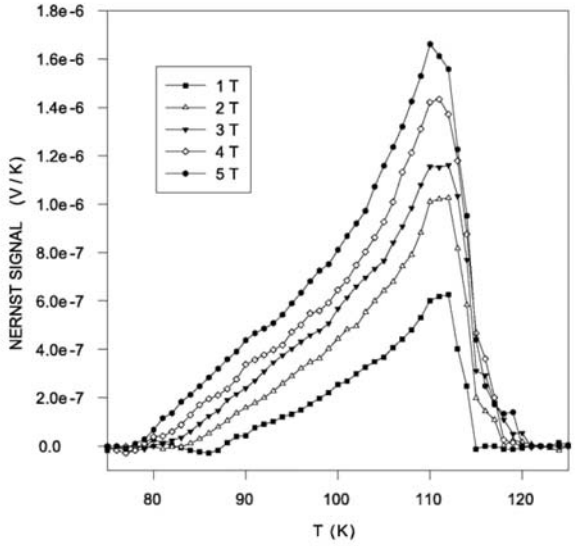

Fig. 4. *Temperature variation of the thermal Hall angle measured in various magnetic fields.*

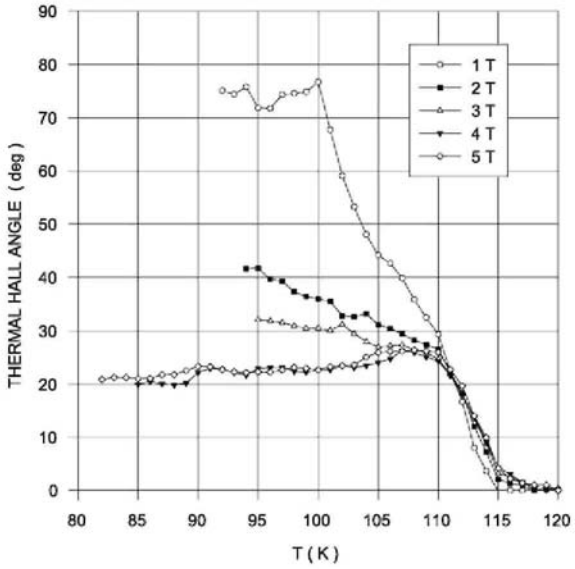

Fig. 5. *Transport entropy as a function of temperature for various magnetic fields.*

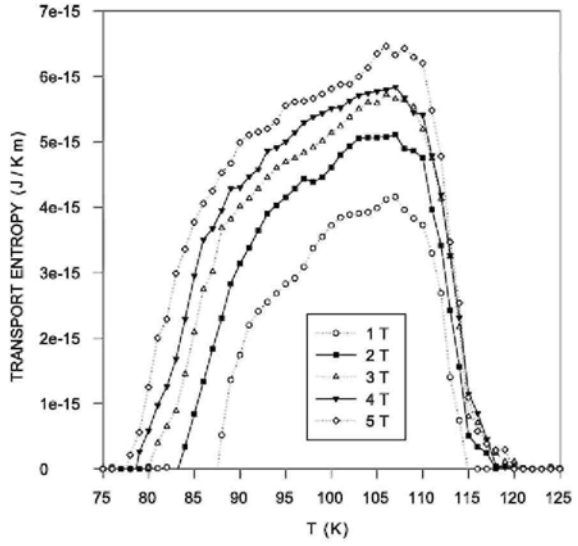

Published in: Physica C-Superconductivity and its Applications (2003), vol. 387, iss. 1-2, pp. 191-197
Status: Postprint (Author's version)

4.4. Thermal conductivity

In the normal state the thermal conductivity increases roughly linearly with temperature (Fig. 6). Below the critical temperature a usual cusp is observable in the thermal conductivity. In a 5 T magnetic field the thermal conductivity in the system is reduced by a factor of 1-2% when compared to the zero field values. Below 109 K the thermal conductivity increases. The difference between 0 and 5 T values becomes about double that of the normal state. This increase of thermal conductivity below T_c is related to reduced phonon scattering, which is typically observed in various high temperature superconductors [14].

The Wiedemann-Franz law allows an estimate of the upper limit of the electronic contribution, k_e, to the thermal conductivity within a free electron approximation through

$$k_e(T) = L_0 T/\rho(T) \qquad (4)$$

where $L_0 = 2.45 \times 10^{-8}$ WΩK^{-2} is the Lorentz number. The electrical resistivity data show that $k_e(T)$ contributes to only about 17% of the thermal conductivity measured in the conductive phase below 200 K, the prevailing part of heat is transported by phonons. This result is comparable to values reported for other typical high temperature superconductors [15].

Fig. 6. *Temperature variation of the thermal conductivity measured in 0 and 5 T magnetic fields.*

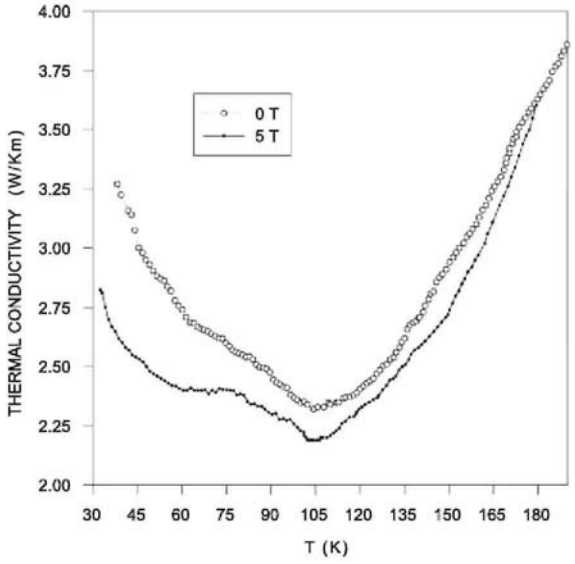

4.5. AC magnetic susceptibility

Comparison of AC susceptibility (Fig. 7) and resistance measurements shows that magnetic shielding occurs below 110 K, i.e. at the temperature where the resistance vanishes and a bulk percolation path is established throughout the whole sample. Therefore the magnetic shielding is mainly caused by intergrain currents and is representative of the grain boundaries within the sample. Two distinct drops of the in-phase AC susceptibility can be seen; a corresponding peak appearing in the out-of-phase signal accompanies each one of them. This reveals the presence of two kinds of grain boundaries or grain connections. The peak occurring between 60 and 80 K is thought to be caused by the Bi-2212 phase intergrowth at the grain boundaries. No traces of other low temperature transitions, related to minority phases, are observed below 60 K.

Published in: Physica C-Superconductivity and its Applications (2003), vol. 387, iss. 1-2, pp. 191-197
Status: Postprint (Author's version)

Fig. 7. *Temperature variation of the AC susceptibility.*

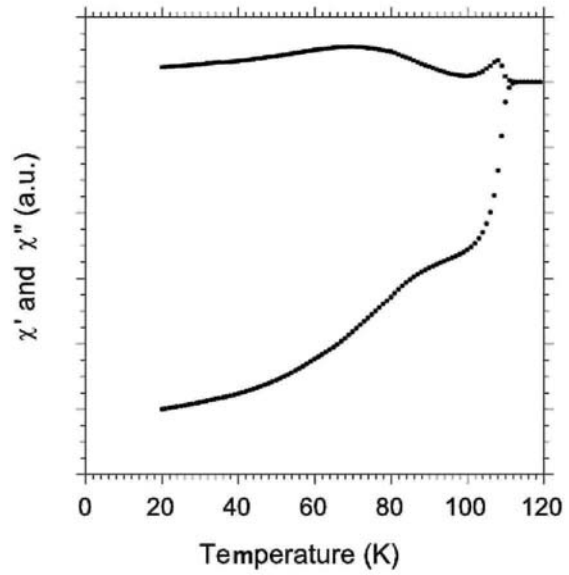

4.6. DC magnetization

Magnetic moment, *M-H* loops, were measured at several temperatures between 20 and 85 K.

From these data (Fig. 8) we have extracted the magnetic irreversibility field H_{irr} defined as the field for which the difference between the upper and lower branches of the magnetic moment loop is smaller than 10^{-6} Am^2. The temperature dependence of the irreversibility field was fit to $\mu_0 H_{irr} = 29.5(1 - T/T_c)^{4.9}$, where T_c was chosen to be equal to 110 K. The fit parameters are similar to those obtained for textured Bi-2223 tapes.

Fig. 8. *Magnetic irreversibility line.*

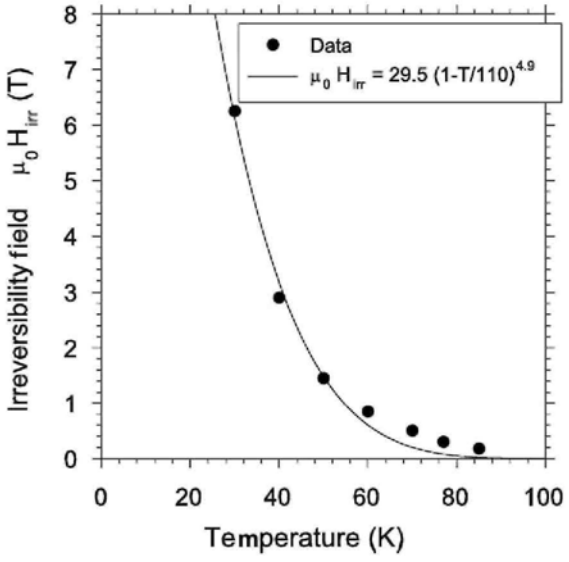

5. Conclusion

The examined niobium doped Bi/Pb2223 superconductor exhibits a high transition temperature (109 K) with a narrow transition interval in the absence of a magnetic field. The magneto-transport properties confirm the crystallographic and microstructure analysis data, i.e. the partial ordering of platelet shaped grains improving the topological intergrain connectivity. It is expected that a modification of preparation and treatment conditions may lead to samples with yet better quality.

The three measured magneto-transport parameters exhibit a different dependence on magnetic field strength as shown in Fig. 9 where the integrated area below the excess curve ($DQ(T,H) = Q(T, H) - Q(T, 0)$) is plotted. The

area below the excess resistivity curve (A_ρ) varies as $A_\rho \sim H^{0.45\pm0.007}$ whereas the area below the excess thermoelectric power, and that below the Nernst effect curves, depend roughly linearly on the magnetic field strength. This can be compared to previously reported data, emphasizing the value of the exponent in the $A_Q \sim H^\alpha$ relation as a signature of the effective dimensionality of the system [16,17]. Such a variety in magnetic and temperature dependencies shows that various mechanisms contribute to electrical resistivity, thermoelectric power, and Nernst effects.

Fig. 9. *Magnetic field dependencies of the excess resistivity, thermoelectric power, and Nernst signals.*

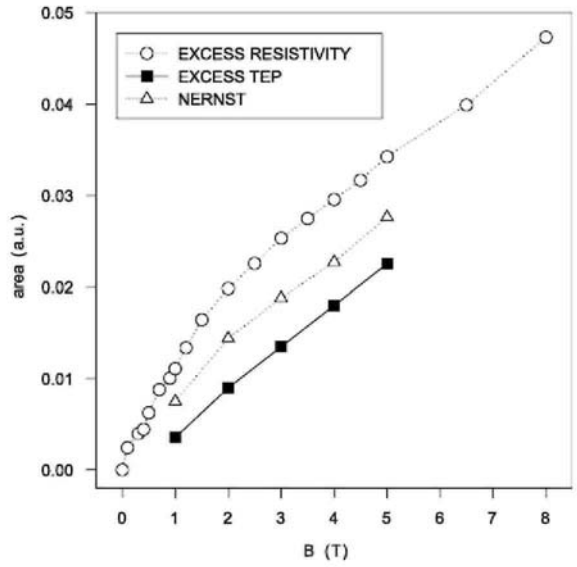

Acknowledgements

Work supported in part by grants 7T08A 02820 and P03B 12919 of the Polish Committee of Scientific Research, PST.CLG.977377of NATO, and by contracts RW 991454 and RW 0114881-VESUVE. Ph. Vanderbemden is a FNRS grantee.

References

[1] S. Stassen, A. Vanderschueren, N. Mazéas, A. Rulmont, M. Ausloos, R. Cloots, Physica C 262 (1996) 45.

[2] S. Stassen, P. Rouxhet, A. Vanderschueren, R. Cloots, A. Rulmont, M. Ausloos, in: U. Balachandran, P.J. McGinn, J.S. Abell (Eds.), High Temperature Superconductors: Synthesis, Processing, and Large-scale Applications, TMS, Warrendale, 1996, p. 113.

[3] S. Stassen, A. Rulmont, M. Ausloos, R. Cloots, Physica C 270 (1996) 135.

[4] B. Robertz, H. Bougrine, A. Rulmont, M. Ausloos, R. Cloots, CIMTEC'98 Proceedings, Adv. Sci. Technol. (Techna, Faenza, 1999), 23 (Science and Engineering of HTC Superconductivity) p. 347.

[5] R. Cloots, B. Robertz, F. Auguste, A. Rulmont, H.Bougrine, N. Vandewalle, M. Ausloos, Mater. Sci. Eng. B 53 (1998) 154.

[6] H. Bougrine, M. Ausloos, M. Pekala, B. Robertz, R. Cloots, Supercond. Sci. Technol. 11 (1998) 803.

[7] Y. Kusano, K. Yamaguchi, M. Fukuhara, A. Doi, T. Takada, M. Fujiwara, J. Takada, J. Jpn. Powder Powder Metall. 38 (1991) 1043.

[8] D. Sykorova, O. Smrckova, P. Vasek, Int. J. Mod. Phys. B 13 (1999) 3738.

[9] O. Smrckova, D. Sykorova, P. Vasek, Int. J. Mod. Phys. B 12 (1998) 3335.

[10] J. Mucha, M. Ausloos, H. Bougrine, R. Cloots, M. Houssa, S. Stassen, M. Pekala, Molec. Phys. Rep. 15-16 (1996) 265.

[11] M. Pekala, H. Bougrine, T. Lada, A. Morawski, M. Ausloos, Supercond. Sci. Technol. 8 (1995) 726.

[12] M. Pekala, W. Gadomski, J. Szydlowska, A. Tampieri, M. Ausloos, Supercond. Sci. Technol. 13 (2000) 1142.

[13] J.L. Tallon, C. Bernhard, H. Shaked, R.L. Hitterman, J.D. Jorgensen, Phys. Rev. B 51 (1995) 12911.

[14] M. Ausloos, in: M. Kazimierski (Ed.), Proc. 11th Seminar of Phase Transitions and Critical Phenomena, Phys. Chem. Solids Series, ILTSR-PAN, Wroclaw, 1998, p. 44.

[15] C. Uher, W.-N. Huang, Phys. Rev. B 40 (1989) 2694.

[16] M. Pekala, M. Ausloos, Physica C 235-240 (1994) 1385.

[17] M. Ausloos, Mol. Phys. Rep. 24 (1999) 158.